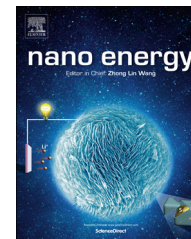




Available online at www.sciencedirect.com

ScienceDirect

journal homepage: www.elsevier.com/locate/nanoenergy



RAPID COMMUNICATION

Efficient photocatalytic H₂ evolution catalyzed by an unprecedented robust molecular semiconductor {Fe₁₁} nanocluster without cocatalysts at neutral conditions



Xiaoqiang Du^{a,1}, Jinli Zhao^{a,1}, Jiaqi Mi^{c,1}, Yong Ding^{a,b,*},
Panpan Zhou^a, Baochun Ma^a, Junwei Zhao^{d,*}, Jie Song^{e,*}

^aKey Laboratory of Nonferrous Metals Chemistry and Resources Utilization of Gansu Province, State Key Laboratory of Applied Organic Chemistry and College of Chemistry and Chemical Engineering, Lanzhou University, Lanzhou 730000, PR China

^bState Key Laboratory for Oxo Synthesis and Selective Oxidation, Lanzhou Institute of Chemical Physics, Chinese Academy of Sciences, Lanzhou 730000, PR China

^cDepartment of Chemistry, Georgia State University, Atlanta, Georgia 30303, USA

^dHenan Key Laboratory of Polyoxometalate Chemistry, College of Chemistry and Chemical Engineering, Henan University, Kaifeng, Henan 475004, PR China

^eDepartment of Biomedical Engineering, Emory University and Georgia Institute of Technology, Atlanta, Georgia 30322, USA

Received 30 March 2015; received in revised form 7 June 2015; accepted 23 June 2015

Available online 9 July 2015

KEYWORDS

Polyoxometalate;
Molecular semiconductor;
Photocatalysis;

Abstract

An unprecedented molecular polyanionic metal oxide cluster of eleven-Fe^{III} substituted antimonotungstate Na₂₇[Fe₁₁(H₂O)₁₄(OH)₂(W₃O₁₀)₂(α-SbW₉O₃₃)₆] · 103H₂O(1) based on earth abundant elements has been successfully synthesized. A careful physical investigation of this molecule reveals that VB = -6.34 eV/CB = -4.39 eV, this unique physical properties ensures that 1 can be defined as a new type of nanoscale molecular semiconductor. This compound

*Corresponding authors.

E-mail addresses: dingyong1@lzu.edu.cn (Y. Ding), zhaojunwei@henu.edu.cn (J. Zhao), jsong7@emory.edu (J. Song).

¹These authors contributed equally to this work.

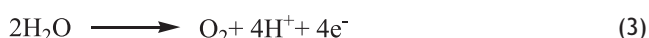
Hydrogen evolution;
Stability

showed remarkable catalytic property for light driven H₂ evolution activity. A H₂ evolution rate of 820 μmol h⁻¹ g⁻¹ was achieved in the presence of **1** without adding any co-catalyst at neutral condition, which is a very high rate among all polyoxotungstate photocatalysts reported thus far. Six evidences proved that **1** is a true stable molecular catalyst during the photocatalytic hydrogen evolution.

© 2015 Elsevier Ltd. All rights reserved.

Introduction

Replacing fossil fuels by an energy system that employs sustainable, green, and safe energy sources is among the greatest technological challenge on this planet. In this context, the production of H₂ via water splitting by sunlight (Eq. (1)) is envisioned as one of the most promising approaches with regard to energy security and sustainability, and also to avoid CO₂ emissions. Water splitting consists of two half reactions (Eqs. (2) and (3)), the reduction and oxidation of water to give hydrogen and molecular oxygen, respectively.



The development of efficient catalysts for hydrogen evolution in the final large scale production driven by visible light is the central topic in artificial photosynthesis [1]. In order to be economically viable, the catalysts should be made from earth abundant materials. So far, hydrogen evolution catalysts of cobalt [2-5], manganese [6], nickel [7,8], iron [9-11], niobium [12,13] and thallium [14] have been reported. Interestingly, it is worth to mention that iron is the most abundant element among all transition metals on the earth and development of iron-based catalysts are intriguing regarding its lower cost, higher eco-benignity, and low-to-zero toxicity in comparison with other extensively used transition metals. Therefore, design and development of catalysts using iron metals as the redox centers for efficient hydrogen production are of great value. For the specific case of well-defined iron-based catalysts, only handful examples were reported for hydrogen evolution.

Our aim is to combine advantages of stability and efficiency as a whole in one catalytic species. Insight into the way how the catalysts function at the molecular level can provide essential information to accelerate the discovery process. Therefore, design and development of molecular level catalysts would potentially benefit the understanding of the electronic nature and inherent catalytic activity of these materials because their structural parameters including compositions, as well as size and charges, can be finely-tuned at molecular level. Polyoxometalates (POMs) are a large class of well-defined transition metal oxide clusters and have unmatched range of physical and chemical properties, which has been widely explored in catalysis, materials science, medicine and nanotechnology [15-20].

Herein, we report a novel molecular polyanionic cluster of eleven-Fe^{III} substituted antimoniotungstate

Na₂₇[Fe₁₁(H₂O)₁₄(OH)₂(W₃O₁₀)₂(α-SbW₉O₃₃)₆] · 103H₂O (**1**) (Figure 1). This iron-containing polyoxometalate (POM), which could be defined as a new molecular semiconductor based on its physical property, is the first example for exceptional photocatalytic hydrogen evolution catalysis for antimoniotungstate. This iron-containing polyoxometalate (POM) exhibits photocatalytic H₂ evolution activity. Under the optimal conditions, a H₂ evolution rate of 820 μmol h⁻¹ g⁻¹ was achieved over **1** without any photosensitizers and co-catalysts at neutral conditions. Eleven-Fe^{III} substituted polyoxometalate of **1** can be conveniently and reproducibly synthesized using simple iron salt of FeCl₃ and trilacunary Keggin-ligand of Na₉[α-SbW₉O₃₃] in aqueous solution. The structure of **1** was confirmed by multiple characterizations including X-Ray, X-ray photoelectron spectroscopy (XPS), Thermal weight analysis (TGA), scanning electron microscopy (SEM), IR, UV-vis diffuse reflectance spectra and elemental analysis.

Results and discussion

Crystallographic data and structural refinements of **1** are summarized in Table S1 (Figures S1-S3, Tables S1-S3). There are multiple intriguing structural features in this crystal. The anionic skeleton of **1** consists of an unique eleven-Fe^{III} substituted gigantic aggregate [Fe₁₁(H₂O)₁₄(OH)₂(W₃O₁₀)₂(α-SbW₉O₃₃)₆]²⁷⁻ (**1a**) (Figure 1a) that is constructed by six trilacunary Keggin [α-SbW₉O₃₃]⁹⁻ fragments linked by an electrophilic [Fe₁₁(H₂O)₁₄(OH)₂(W₃O₁₀)₂]²⁷⁺ cluster unit. To the best of our knowledge, such particular eleven-Fe^{III} substituted gigantic aggregate with a nanoscale size of 1.75 × 2.48 × 2.50 nm³ is for the first time observed in polyoxometalate chemistry and a rare example in coordination chemistry. Interestingly, the distribution motif of the six segments resembles the *chair* configuration of cyclohexane in its low energy form (Figure 1b), and similar *chair* configuration has been observed in a hexameric tungstoarsenate [As₆W₆₅O₂₁₇(H₂O)₇]²⁶⁻ reported by Kortz [21] in 2001. Considering the charge balance and the reaction conditions, two protons are directly added to the formula of **1**. In order to locate the possible positions of these two protons and fourteen coordination water molecules in **1a**, bond valence sum (BVS) calculations of all oxygen atoms in **1a** have been performed (Table S4). [22] The BVS value (1.09) of O94/O94A (symmetrical code A: -x, 1-y, 1-z) atoms is significantly lower than 2, indicative of two possible positions binding protons (Figures 2a and 3a). The BVS values of O1W/O1WA, O2W/O2WA, O3W/O3WA, O4W/O4WA, O5W/O5WA, O6W/O6WA and O7W/O7WA

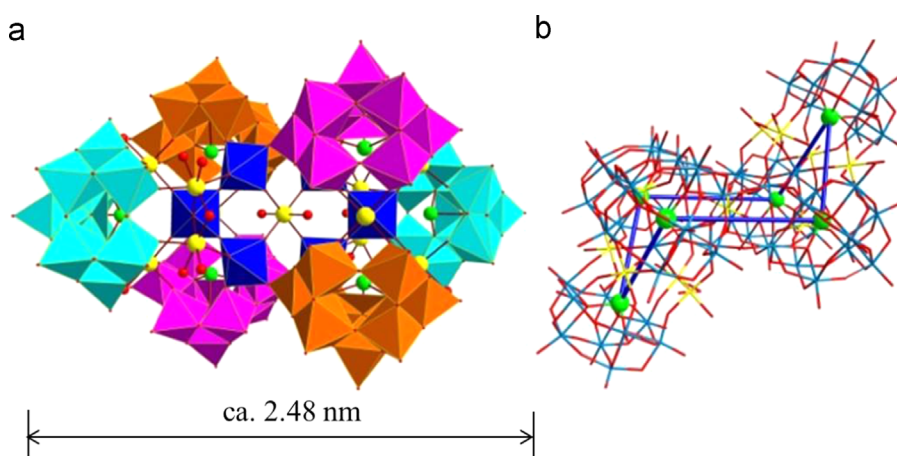


Figure 1 (a) Combined polyhedral/ball-and-stick representation of **1a**; (b) The chair-like configuration of **1a**. Color scheme: $[\alpha\text{-SbW}_9\text{O}_{33}]^{9-}$ polyhedra (turquoise, pink, orange), the bridging WO_6 octahedra (blue), Fe (yellow), O/H₂O/OH (red), Sb (bright green).

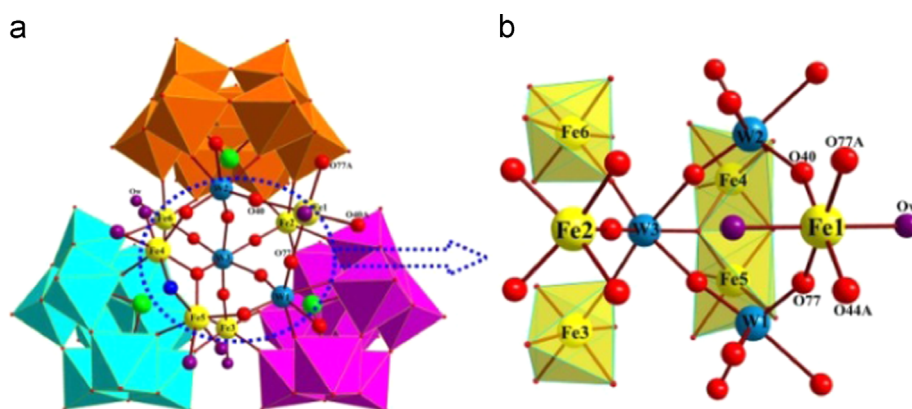


Figure 2 (a) Combined polyhedral/ball-and-stick representation of the $[\text{Fe}_{5.5}(\text{H}_2\text{O})_7(\text{OH})(\text{W}_3\text{O}_{10})(\alpha\text{-SbW}_9\text{O}_{33})_3]^{13.5-}$ half-unit of **1a**; (b) the $[\text{Fe}_{5.5}(\text{H}_2\text{O})_7(\text{OH})(\text{W}_3\text{O}_{10})]^{13.5+}$ core in the trimeric $[\text{Fe}_{5.5}(\text{H}_2\text{O})_7(\text{OH})(\text{W}_3\text{O}_{10})(\alpha\text{-SbW}_9\text{O}_{33})_3]^{13.5-}$ half-unit. The atoms with "A" in their labels are symmetrically generated (A: -x, 1-y, 1-z). Color scheme: $[\alpha\text{-SbW}_9\text{O}_{33}]^{9-}$ polyhedra (turquoise, pink, orange), Fe (yellow), O (red), H₂O (violet), OH (blue), Sb (bright green), W (light blue).

are 0.42, 0.34, 0.41, 0.42, 0.45, 0.38 and 0.34, respectively, which suggest that these positions are occupied by water ligands (Figures 2a and 3a). In addition, BVS calculations show that the valences of all iron atoms in **1a** are +3 (Supplementary information). Moreover, the XPS result (Figure S9) further consolidates the assignment of the valences in all iron atoms.

It is noteworthy that the eleven-Fe^{III} substituted aggregate **1a** is centrosymmetric and can be regarded as a combination of two crystallographically equivalent $[\text{Fe}_{5.5}(\text{H}_2\text{O})_7(\text{OH})(\text{W}_3\text{O}_{10})(\alpha\text{-SbW}_9\text{O}_{33})_3]^{13.5-}$ half-units (Figure 2a) related by an inversion center (Fe1) with the atomic coordinate of (0, 0.5, 0.5) through Fe1 and four W-O-W connectors. In the $[\text{Fe}_{5.5}(\text{H}_2\text{O})_7(\text{OH})(\text{W}_3\text{O}_{10})(\alpha\text{-SbW}_9\text{O}_{33})_3]^{13.5-}$ half-unit, each of the Fe2, Fe6 and W2 centers are connected with two lacunary oxygen atoms from one $[\alpha\text{-SbW}_9\text{O}_{33}]^{9-}$ fragment (as shown in orange). The Fe3, Fe4, Fe5 and Fe6 ions are in junction with six lacunary oxygen atoms from the other $[\alpha\text{-SbW}_9\text{O}_{33}]^{9-}$ fragment (as shown in turquoise) where each of the Fe4 and Fe5 ions only links one lacunary oxygen atom. While each of the Fe3 and Fe6 cations are combined with one lacunary oxygen atom, and each of the Fe2, Fe3 and W1 atoms join to

two lacunary oxygen atoms from the third $[\alpha\text{-SbW}_9\text{O}_{33}]^{9-}$ fragment (as shown in pink). Then Fe2, Fe3, Fe4, Fe5, Fe6, W1 and W2 centers are bridged together by the W3 atom. At the meantime, the Fe1 atom concatenates the W1 and W2 atoms, thus giving rise to the windmill-shaped trimeric $[\text{Fe}_{5.5}(\text{H}_2\text{O})_7(\text{OH})(\text{W}_3\text{O}_{10})(\alpha\text{-SbW}_9\text{O}_{33})_3]^{13.5-}$ half-unit, which is completely distinct from the recently reported windmill-shaped trimeric Gd^{III}-substituted germanotungstate fragment in $\text{Na}_3\text{H}_7[\text{Cu}(\text{en})_2]_5[\text{Cu}(\text{en})(\text{H}_2\text{O})_2][\text{Gd}_4\text{Ge}_4\text{W}_{46}\text{O}_{164}(\text{H}_2\text{O})_3] \cdot 25\text{H}_2\text{O}$ [23]. It should be pointed out that Fe2, Fe3 and Fe6 cations also play an important connection role in the construction of the trimeric half-unit, in which each of Fe2, Fe3 and Fe6 cations simultaneously bridge two adjacent $[\alpha\text{-SbW}_9\text{O}_{33}]^{9-}$ fragments together. Another intriguing feature is that the Fe1 cation concurrently links the W1 and W2 centers forming a rare $\{\text{W}_3\text{FeO}_4\}$ eight-member ring to enhance the chemical stability of this cluster (Figure 2b).

The most remarkable construction trait of **1a** is that there is an eleven-Fe^{III} containing electrophilic $[\text{Fe}_{11}(\text{H}_2\text{O})_{14}(\text{OH})_2(\text{W}_3\text{O}_{10})_2]^{27+}$ cluster unit (Figure 3a). In this $\{\text{Fe}_{11}\}$ cluster unit, there are two kinds of coordinate geometries for the iron ions. The Fe2 cation is

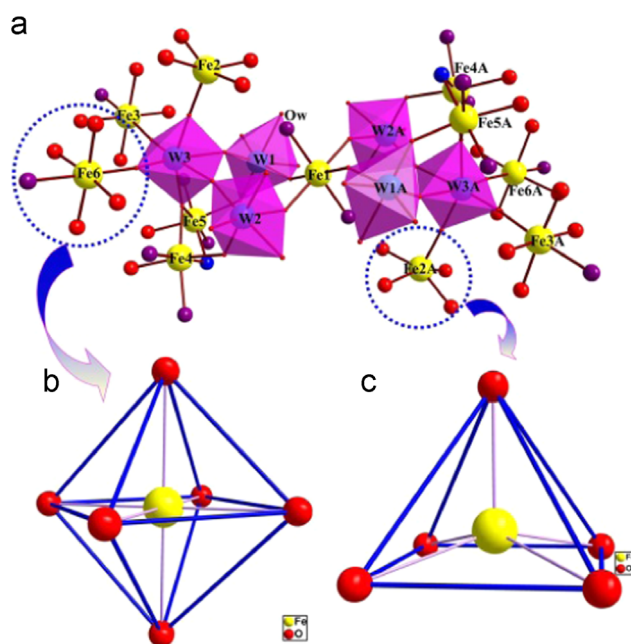


Figure 3 (a) Combined polyhedral/ball-and-stick representation of the electrophilic $[\text{Fe}_{11}(\text{H}_2\text{O})_{14}(\text{OH})_2(\text{W}_3\text{O}_{10})_2]^{27+}$ cluster in **1a**; (b) the octahedral configuration of the hexa-coordinate Fe^{3+} cations; (c) the square pyramidal geometry of the penta-coordinate Fe^{3+} cation. Color scheme: Fe (yellow), O (red), H_2O (violet), OH (blue).

five-coordinate and the remaining are six-coordinate (Figure 3b and c). Specifically speaking, the octahedral Fe1 ion is defined by four oxygen atoms from four WO_6 octahedra for the basal plane [Fe-O: 1.948(16)-1.951(14) Å] and two oxygen atoms from two water ligands for two axial positions [Fe-Ow: 2.081(14) Å]. The Fe2 cation resides in a square pyramid established by one oxygen atom from the W_3O_6 octahedron [Fe-O: 1.844(18) Å] and four oxygen atoms from two adjacent trilacunary Keggin $[\alpha\text{-SbW}_9\text{O}_{33}]^9$ fragments [Fe-O: 1.930(17)-1.983(17) Å]. The Fe3 and Fe6 cations exhibit the octahedral geometries in which four oxygen atoms from two adjacent $[\alpha\text{-SbW}_9\text{O}_{33}]^9$ fragments constitute the basal plane [Fe3-O: 1.956(16)-1.992(19) Å] and [Fe6-O: 1.978(19)-2.020(15) Å], and one O atom from the W_3O_6 octahedron [Fe3-O: 1.955(17) Å, Fe6-O: 1.971(16) Å] and a water ligand [Fe3-Ow: 2.161(17) Å, Fe6-Ow: 2.163(16) Å] occupy two axial sites. The octahedral Fe4 and Fe5 cations are edge-shared *via* a OH and a $\mu_3\text{-O}$ groups and their octahedral coordination spheres are completed by two water ligands [Fe-Ow: 2.057(18)-2.116(17) Å], two $\mu_2\text{-O}$ atoms from W_2O_6 or W_1O_6 octahedra and $[\alpha\text{-SbW}_9\text{O}_{33}]^9$ fragments [1.981(15)-1.986(17) Å], one $\mu_3\text{-O}$ atom from W_3O_6 octahedron [Fe-O: 2.026(15)-2.073(14) Å] and a OH group [Fe-O: 1.983(17)-1.986(17) Å].

X-ray photoelectron spectroscopy (XPS) of Fe 2p in compound **1** (Figure S9) displays the binding energy regions of Fe 2p_{3/2} and Fe 2p_{1/2} peaks at 711.5 eV and 725.4 eV, respectively. The 13.9 eV difference between Fe 2p_{3/2} and Fe 2p_{1/2} peaks and the presence of a satellite peak at near 720.3 eV are characteristics of Fe (^{III}) in {Fe₁₁} cluster [24]. To

determine the relative positions of valence band (VB) and conduction band (CB) edges, the highest occupied molecular orbital (HOMO) and lowest unoccupied molecular orbital (LUMO) levels are calculated from the ionization potentials (Figure S26) and by assuming the energy level relative to that normal hydrogen electrode (NHE) potential is -4.5 eV below the vacuum level [25]. The UV-vis diffuse reflectance spectrum of **1** revealed that the band gap (E_g) (Figures S10 and S11) of **1** was approximately 1.95 eV (VB = -6.34 eV and CB = -4.39 eV). As soluble metal oxides, the electronic and light-absorption characteristics of POMs are also similar to metal oxide semiconductors (MOSs) because of the similarities in composition and structure. For instance, VB and CB in MOSs are equivalent to the HOMO and the LUMO of POMs, respectively. Upon irradiation, electrons in POMs are promoted from the low-energy electronic states to the high-energy electronic states, as from the VB that are mainly comprised of oxygen 2p orbitals to CB in the band model that are mainly comprised of metal d orbitals in MOSs. However, no definition of polyoxometalate as a molecular semiconductor has been reported so far. In addition, molecule **1** exhibits an intrinsic conductivity of $1.1 \times 10^{-4} \Omega^{-1} \text{cm}^{-1}$ as measured by conductivity meter, which is in the semiconductor range [26]. Under a certain temperature, production and recombination of electron-hole exist at the same time and achieve a dynamic balance; the intrinsic semiconductor has certain carrier concentration exhibiting the electrical conductivity.

Based on the above analysis, molecule 1 can be defined as a molecular semiconductor.

Light-driven hydrogen evolution was thoroughly investigated in neutral aqueous solution containing triethanolamine (TEOA) as the sacrificial electron donor (TEOA/H₂O, V/V=5/95, pH=7.0, concentrated HCl was used to adjust the solution as neutral medium). Compound 1 demonstrated remarkable photocatalytic activity for hydrogen production.

H₂ evolution rate of as high as 820 μmol h⁻¹ g⁻¹ was achieved under the optimized conditions. Photocatalytic hydrogen evolution was first examined under different concentrations of 1 (Figure 4). The maximum amount of H₂ formation was obtained when the concentration of 1 was 60 μM. Photogenerated electrons that derived from the excited state of Fe₁₁-POM might be insufficient under lower concentrations of 1 (less than 60 μM) in which process the H⁺ was reductive to H₂, resulting in the poor activity of hydrogen evolution. On the contrary, a decreased activity for hydrogen evolution was observed when high catalyst concentrations (more than 60 μM) were used. Therefore, 60 μM of 1 was used for further optimization of the hydrogen evolution.

We also tested the dependence of photocatalytic hydrogen production activity on the TEOA concentrations (Figure 5). The reaction gave the highest amount of hydrogen evolution when the concentration ratio of TEOA/H₂O is 5: 95 (V/V). The activity of hydrogen evolution reaction was substantially affected by the electron-donating ability of the sacrificial reagent. A series of control experiments were conducted for photocatalytic hydrogen evolution. No hydrogen was detected when the photocatalytic reaction was carried out in pure water, indicating that the sacrificial electron donor is an indispensable component. No hydrogen was detected without light irradiation for 1 and TEOA solution, indicating the reaction of H₂ evolution is only driven by light (Table S7). Under the optimized condition, that is 60 μM of 1 in the aqueous TEOA solution (TEOA/H₂O, V/V=5/95) at pH 7.0 (Figure 6), compound 1 demonstrated

remarkable photocatalytic activity for H₂ evolution. In the continuous three-run reaction, the H₂ production rates of 1 can arrive at 820, 802, and 786 μmol h⁻¹ g⁻¹, irrespectively. The total amount of H₂ for 12 h is 938 μmol with a TON of 156 and TOF of 13 h⁻¹. No obvious change of the hydrogen evolution rate was detected within 12 h (Figures 6 and S22). In our unique photocatalytic H₂ evolution system, it should be noted that no Pt source or other cocatalysts such as Eisenberg's cobaloximes [13] was used, which is completely different from other reported hydrogen production system. Especially, TEOA is the first example as the sacrificial electron donor for the hydrogen evolution over POM under the UV light illumination. This H₂ evolution rate of 1 is moderately comparable to that of the {Ta₁₂} cluster

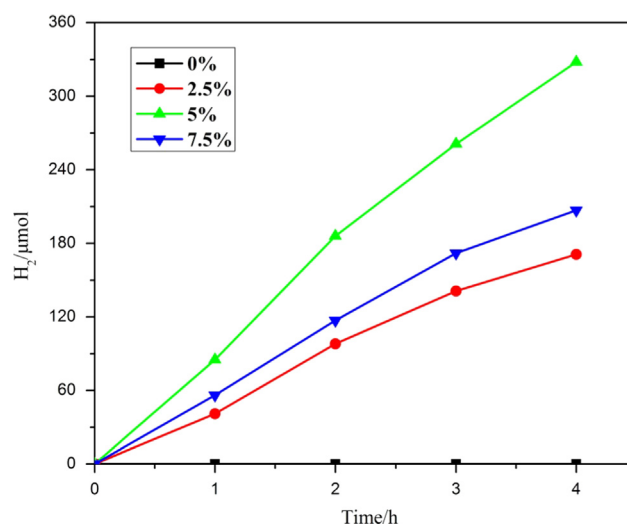


Figure 5 Effect of TEOA amount on the hydrogen evolution. 1 (60 μM) was dissolved in 100 mL 0%, 2.5%, 5%, 7.5% TEOA/H₂O (V/V) (pH=7.0) solution in a quartz cell. Other conditions were the same as in Figure 4.

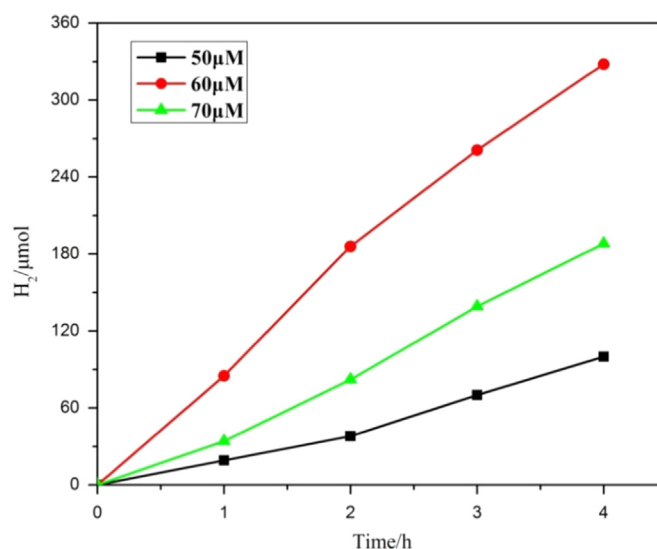


Figure 4 Hydrogen production over different concentrations of 1. 1 (50, 60, 70 μM) was dissolved in 100 mL 5%TEOA/H₂O (V/V) (pH=7.0, concentrated HCl was used to adjust the solution as neutral medium) solution in a quartz cell. The reaction solution was irradiated under a 250 W high pressure mercury lamp.

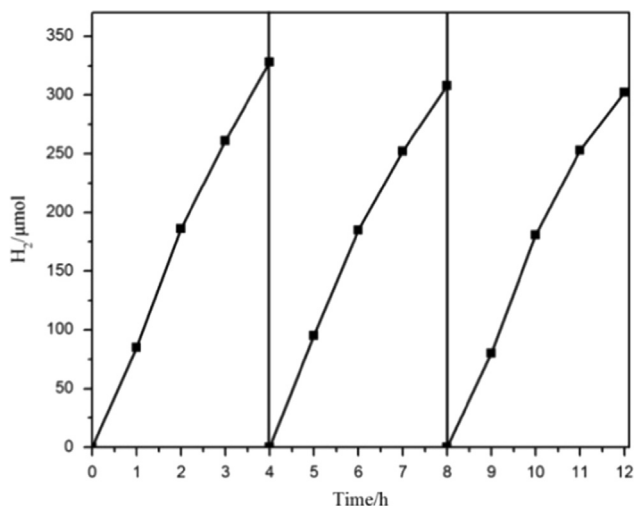


Figure 6 Time course of photocatalytic H₂ evolution in presence of **1** (60 μM) in TEOA/H₂O (100 mL, V/V=5/95, pH=7.0) solution. Other conditions were the same as in Figure 4.

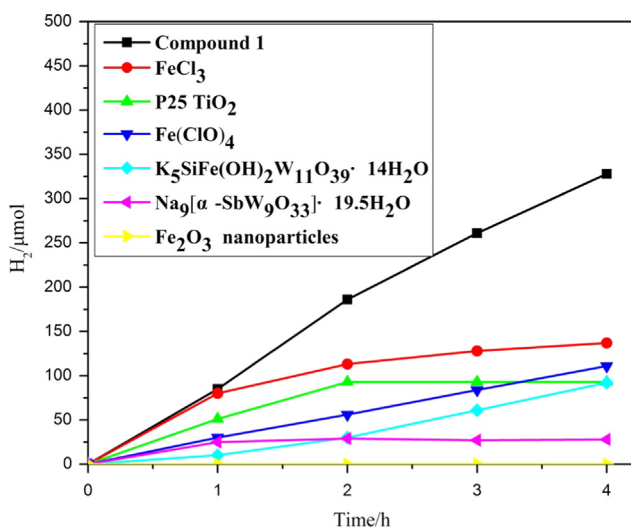


Figure 7 The time course of H₂ evolution over different catalysts. Conditions: Black: 6 μmol Compound **1**; Red: 66 μmol FeCl₃; Green: 117 mg P25 TiO₂; Blue: 66 μmol Fe(ClO₄)₃; Cyan: 66 μmol K₅SiFe(OH)₂W₁₁O₃₉·14H₂O; Magenta: 36 μmol Na₉[α-SbW₉O₃₃]·17H₂O; Yellow: 33 μmol Fe₂O₃ nanoparticles. Other conditions were the same as in Figure 4.

containing polytantalotungstates in the presence of H₂PtCl₆ under UV illumination, which is the highest among all polyoxotungstate photocatalysts reported thus far reported by Liu [14].

Multiple control experiments were performed in the presence of simple iron salts (FeCl₃ and Fe(ClO₄)₃), iron oxide nanoparticles (Fe₂O₃ nanoparticles), typical semiconductor P25 TiO₂, iron-containing POM (K₅SiFe(OH)₂W₁₁O₃₉·14H₂O), and the POM without irons (Na₉[α-SbW₉O₃₃]·17H₂O) (Figure 7). Under the identical hydrogen evolution conditions, compound **1** exhibits the highest catalytic activity with the H₂ amount of 328 μmol in 4 h (Figure 7). Both FeCl₃ and Fe(ClO₄)₃ showed very low catalytic activities in H₂ evolution producing 137 μmol and 111 μmol H₂, which are almost 2-3 times lower than that of

compound **1**. Interestingly, in the first 1 h, the photocatalytic efficiency of FeCl₃ is similar to the one of **1**. Here, both **1** and FeCl₃ are used at the same equivalent amount of Fe atoms (as is shown in Figure 7 caption). However, FeCl₃ will transform to heterogeneous metal oxide and hydroxide when the reaction continues, so the hydrogen evolution rate became slower compared with that of **1**. Catalyst **1** is stable for photocatalytic hydrogen evolution in the neutral conditions, so the hydrogen production rate remains constant in reaction duration. The superior catalytic activity of **1** should be due to the special coordination environment of Fe atoms. Compared to two POM compounds, either iron-containing K₅SiFe(OH)₂W₁₁O₃₉ or iron-free Na₉[α-SbW₉O₃₃], both POMs showed even much less catalytic activities. α-Fe₂O₃ nanoparticles with size of about 60 nm are catalytically inactive; whereas, P25 TiO₂ show a relatively lower activity. These results indicate that the coordination geometry and condition of Fe elements centered in Fe₁₁-POM cluster plays a significant role in determination of (both the transmission and efficient separation) electrons and holes generation and transfer.

The excellent catalytic activity of **1** in hydrogen production could be ascribed to the following mechanism. First, under the UV light irradiation, electrons in catalyst **1** are excited from O 2p (VB) to Fe 3d (CB). The electrons filled in the 3d⁵ orbital (CB) of Fe^{III} in **1** are half-filled and therefore in the stable state. The 3d⁵ orbital (CB) are not prone to accept those photogenerated electrons. Thereby, the electrons in the CB could easily escape from **1** and become external free electrons [1], resulting in the production of hydrogen. Second, it is well documented that the dipole moment originated from the distortion of metal-O polyhedra plays a key role in electron and hole separation in the photolytic process and consequently the increasing catalytic activities of POMs [14,27]. In compound **1**, two FeO₅ tetragonal pyramids (Figure 3c) are severely distorted due to the space steric effect, which is different from the rest of the nine normal FeO₆ octahedra (Figure 3b). The distortion of FeO₅ square pyramids are clearly evidenced by the Fe-O bond lengths between 1.844(18) Å and 1.983(17) Å and the O-Fe-O bond angles between 85.7° and 155.7°. Third, two μ-OH and fourteen aqua ligands are bonded directly to the Fe^{III} centers in compound **1** (Figures 2a and 3a), resulting in a viable pathway for electron transfer and the subsequent reduction of proton to H₂.

The stability of **1** in photocatalytic hydrogen evolution was thoroughly investigated. First, as shown in Figure 6, kinetics profile of three continuous runs nearly remain the same and H₂ evolution rates are tightly close to each other, indicating that **1** is very stable during photocatalytic process. Second, dynamic light scattering (DLS) study shows that no colloidal nanoparticles can be detected after light illumination, revealing that the photocatalytic hydrogen evolution reaction is a homogeneous system (Figure S23). Third, no change is observed in the UV-vis spectra of **1** in the reaction solution aged over 12 h (Figure 8b), which supports that **1** is stable in the study conditions. Moreover, catalyst aged in the reaction solution for 12 h showed the same photocatalytic H₂ evolution performance as the freshly-prepared one (Figure 9). Fourth, UV-vis spectra of **1** before and after the photocatalysis are identical (Figure S24), suggesting compound **1** remains intact during the H₂

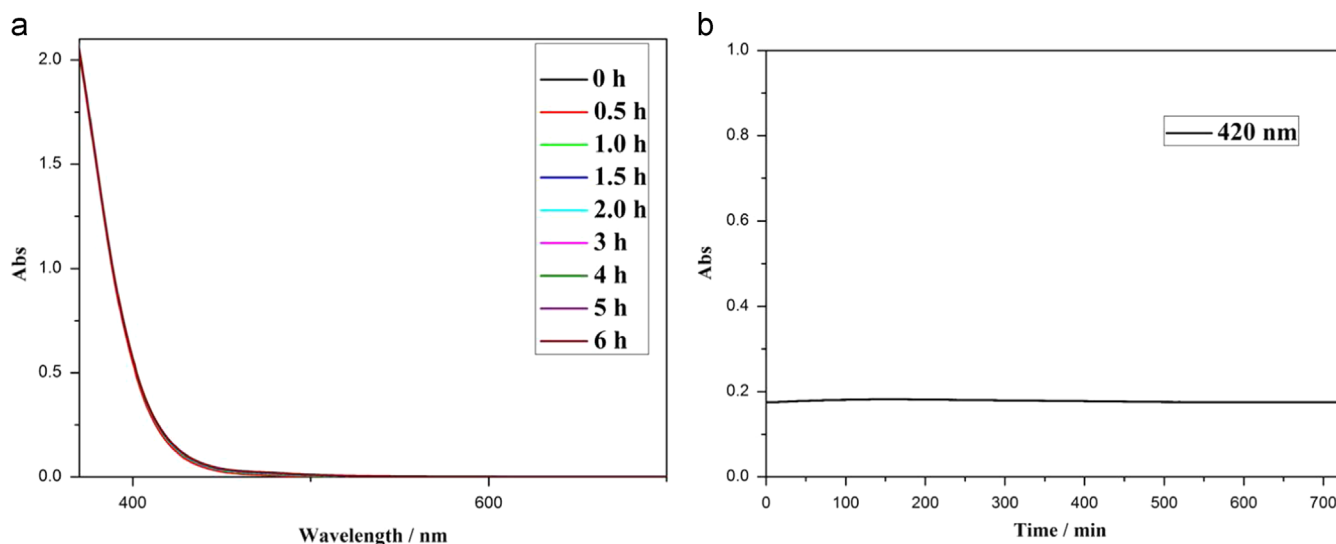


Figure 8 (a) Time-dependent UV-vis absorption spectra of **1** (60 μM) over 6 h, in 5%TEOA/H₂O (V/V) (pH=7.0) solution. (b) Time profile of UV-vis spectra ($\lambda=420$ nm) of **1** (60 μM) in TEOA/H₂O (100 mL, V/V=5/95, pH=7.0) solution over a 12-h period.

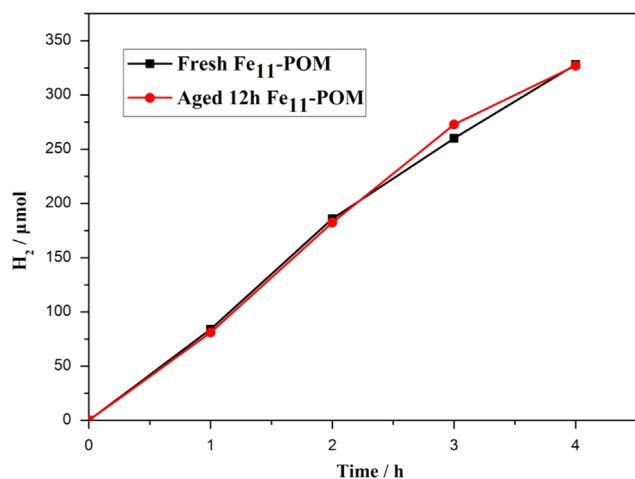


Figure 9 Kinetics of H₂ evolution in the photocatalytic system using freshly-prepared **1** (black) and 12 h-aged **1** (60 μM) (red). The reaction conditions are the same as in Figure 4.

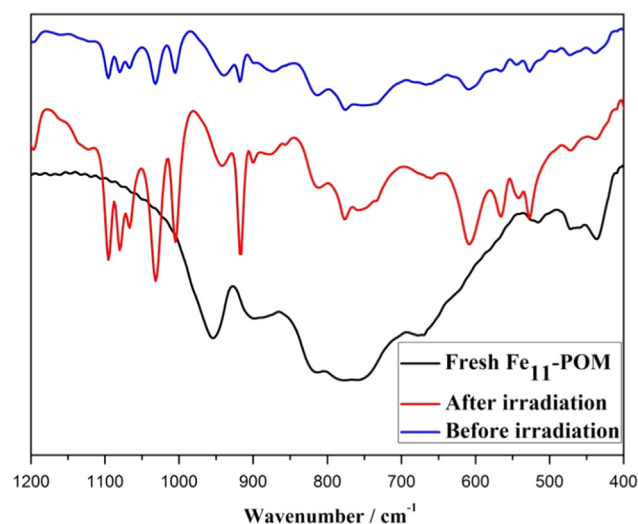


Figure 10 FT-IR spectra of pure **1** (black); **1** (blue) isolated from the reaction solution containing TEOA using [Ru(bpy)₃]²⁺ as the precipitants before light illumination; and **1** (red) isolated from post-catalytic reaction solution after illumination for 4 h.

generation reaction. Fifth, the cyclic voltammograms of **1** in TEOA/H₂O (V/V=5/95, pH=7.0) solution can be reproduced in multiple scans (Figure S25), revealing that **1** is stable during the reversible redox process. Sixth, The FT-IR spectra of Fe₁₁-POM isolated from post-reaction solution after 4 h remain unchanged with comparison to the spectrum before photocatalytic reaction (Figure 10).

To understand the mechanisms of O₂ or H₂ evolution (Figure 11), the electronic band structure of **1** is investigated. UV-vis diffuse reflectance spectrum of **1** (Figure S10) shows that one absorption edge is observed at ca. 635 nm ($E_g=1.95$ eV). Quantum mechanical calculations were further employed to obtain the electronic properties of **1**. The optimized geometry for **1** is depicted in Figure S27. The calculated energies for the highest occupied molecular orbital (HOMO) and the lowest unoccupied molecular orbital (LUMO) are -7.05 and -5.70 eV, respectively. The HOMO-LUMO energy gap is 1.35 eV. It is well known that photocatalytic hydrogen evolution often requires the CB of

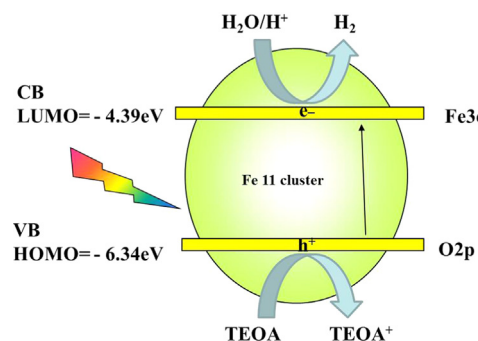


Figure 11 Proposed mechanism for the photocatalytic hydrogen evolution over **1**. CB: conduction band; VB: valence band; LUMO: Lowest Unoccupied Molecular Orbital; HOMO: Highest Occupied Molecular Orbital.

semiconductor to meet the thermodynamic potentials for the reaction, in which the bottom level of the CB should be more negative than the potential of H^+/H_2 (0 V vs. NHE). As for **1**, the CB locates at -4.39 eV (Figure S26), which is more negative than the reduction potential of H^+/H_2 . Therefore, **1** is thermodynamically capable for photocatalytic H_2 production.

Conclusion

In summary, an unprecedented molecular eleven-Fe^{III} substituted antimonotungstate $\text{Na}_{27}[\text{Fe}_{11}(\text{H}_2\text{O})_{14}(\text{OH})_2(\text{W}_3\text{O}_{10})_2(\alpha\text{-SbW}_9\text{O}_{33})_6] \cdot 103\text{H}_2\text{O}$ (**1**) based on earth-abundant elements has been successfully synthesized for the first time and carefully characterized. Our thorough study demonstrates that **1** is an efficient photocatalyst for hydrogen evolution. This eleven-Fe^{III}-containing nanocluster showed remarkable photocatalytic activity for hydrogen production at neutral pH without adding any Pt or other cocatalysts and photosensitizers. Molecule **1** is extremely stable during the turnovers in the photocatalytic hydrogen evolution system. The discovery of the novel iron-based catalysts described herein clearly fill a gap in the design and development of water-splitting systems, which aim to be eventually used in artificial photosynthetic schemes to enable efficient and sustainable solar fuel conversion and storage.

Experimental section

Synthesis of $\text{Na}_{27}[\text{Fe}_{11}(\text{H}_2\text{O})_{14}(\text{OH})_2(\text{W}_3\text{O}_{10})_2(\alpha\text{-SbW}_9\text{O}_{33})_6] \cdot 103\text{H}_2\text{O}$ (**1**)

1.16 g (7.2 mmol) of FeCl_3 was dissolved in 80 mL of H_2O , and then 9.45 g (3.3 mmol) of $\text{Na}_9[\alpha\text{-SbW}_9\text{O}_{33}] \cdot 17\text{H}_2\text{O}$ was added. The pH of the solution obtained was 3.0. Then, the solution was heated to 90°C for 1 h and filtered after cooling to room temperature. Slow evaporation of the clear filtrate at room temperature led to yellow crystals which are suitable for X-ray diffraction within 8–9 days (yield 1.0 g, 10.0%). Thermogravimetric analysis (TGA) gave 103 water molecules of hydration. FT-IR: 953, 896, 818, 765, 676, 518, 480, 432 cm^{-1} . Anal. calcd (Found) for **1**: Na 3.23 (3.14), Fe 3.14 (3.17), Sb 3.92 (3.86), W 59.2 (58.4).

Photocatalytic hydrogen evolution

Photocatalytic hydrogen generation was performed as follows. The desired concentration of catalyst (50–70 μM) was added to 5% TEOA/ H_2O (V/V=5/95, pH=7.0) solution in a quartz cell. The above solution was deaerated by purging with Ar gas for 10 min in a flask (150 mL) sealed with a rubber septum (the volume of reaction solution was 100 mL). The reaction was then started by irradiating the solution with a 250 W high pressure mercury lamp. After each irradiation time, 150 μL of Ar was injected into the flask and then the same volume of gas in the headspace of the flask was withdrawn by a SGE gas-tight syringe and analyzed by gas chromatography (GC).

Acknowledgments

This work was financially supported by the National Natural Science Foundation of China (Grant nos. 21173105, 21172098 and 21101055). We gratefully thank Dr. Shixiong Min and Prof. Changwen Hu for his valuable discussions.

Appendix A. Supplementary information

Supplementary data associated with this article can be found in the online version at <http://dx.doi.org/10.1016/j.nanoen.2015.06.025>.

References

- [1] X. Chen, S. Shen, L. Guo, S.S. Mao, *Chem. Rev.* 110 (2010) 6503.
- [2] T. Lazarides, T. McCormick, P. Du, G. Luo, B. Lindley, R. Eisenberg, *J. Am. Chem. Soc.* 131 (2009) 9192.
- [3] C. Leung, S. Ng, C. Ko, W. Man, J. Wu, L. Chen, T. Lau, *Energy Environ. Sci.* 5 (2012) 7903.
- [4] W.R. McNamara, Z. Han, P.J. Alperin, W.W. Brennessel, P.L. Holland, R. Eisenberg, *J. Am. Chem. Soc.* 133 (2011) 15368.
- [5] J. Zhao, Y. Ding, J. Wei, X. Du, Y. Yu, R. Han, *Int. J. Hydrogen Energy* 39 (2014) 18908.
- [6] H. Lv, J. Song, H. Zhu, Y.V. Geletii, J. Bacsá, C. Zhao, T. Lian, D.G. Musaev, C.L. Hill, *J. Catal.* 307 (2013) 48.
- [7] M.L. Helm, M.P. Stewart, R.M. Bullock, M.R. DuBois, D.L. DuBois, *Science* 333 (2011) 863.
- [8] Z. Han, F. Qiu, R. Eisenberg, P.L. Holland, T.D. Krauss, *Science* 338 (2012) 1321.
- [9] G. Zou, G. Zhang, B. Hu, J. Li, M. Feng, X. Wang, X. Huang, *Chem. Eur. J.* 19 (2013) 15396.
- [10] F. Gärtner, B. Sundararaju, A. Surkus, A. Boddien, B. Loges, H. Junge, P.H. Dixneuf, M. Beller, *Angew. Chem. Int. Ed.* 48 (2009) 9962.
- [11] F. Wang, W. Liang, J. Jian, C. Li, B. Chen, C. Tung, L. Wu, *Angew. Chem. Int. Ed.* 52 (2013) 8134.
- [12] Z. Zhang, Q. Lin, D. Kurunthu, T. Wu, F. Zuo, S.T. Zheng, C.J. Bardeen, X. Bu, P. Feng, *J. Am. Chem. Soc.* 133 (2011) 6934.
- [13] P. Huang, C. Qin, Z. Su, Y. Xing, X. Wang, K. Shao, Y. Lan, E. Wang, *J. Am. Chem. Soc.* 134 (2012) 14004.
- [14] S. Li, S. Liu, S. Liu, Y. Liu, Q. Tang, Z. Shi, S. Ouyang, J. Ye, *J. Am. Chem. Soc.* 134 (2012) 19716.
- [15] D.L. Long, R. Tsunashima, L. Cronin, *Angew. Chem. Int. Ed.* 49 (2010) 1736.
- [16] J.T. Rhule, C.L. Hill, D.A. Judd, R.F. Schinazi, *Chem. Rev.* 98 (1998) 327.
- [17] N. Mizuno, M. Misono, *Chem. Rev.* 98 (1998) 199.
- [18] F. Song, Y. Ding, B. Ma, C. Wang, Q. Wang, X. Du, S. Fu, J. Song, *Energy Environ. Sci.*, 6 (2013) 1170.
- [19] H. Lv, Y.V. Geletii, C. Zhao, J.W. Vickers, G. Zhu, Z. Luo, J. Song, T. Lian, D.G. Musaev, C.L. Hill, *Chem. Soc. Rev.* 41 (2012) 7572.
- [20] S. Zheng, G. Yang, *Chem. Soc. Rev.* 41 (2012) 7623.
- [21] U. Kortz, M.G. Savellieff, B.S. Bassil, M.H. Dickman, *Angew. Chem. Int. Ed.* 40 (2001) 3384.
- [22] I. Brown, D. Altermatt, *Acta Crystallogr. Sect. B* 41 (1985) 244.
- [23] J. Zhao, D. Shi, L. Chen, P. Ma, J. Wang, J. Zhang, J. Niu, *Cryst. Growth Des.* 13 (2013) 4368.
- [24] M. Descostes, F. Mercier, N. Thomat, C. Beaucaire, S.M. Gautier, *Appl. Surf. Sci.* 165 (2000) 288.

- [25] J. Liu, Y. Liu, N. Liu, Y. Han, X. Zhang, H. Huang, Y. Lifshitz, S. Lee, J. Zhong, Z. Kang, *Science* 347 (2015) 970.
- [26] M. Maitrot, G. Guillaud, B. Boudjema, J. Andre, H. Strzelecka, J. Simon, R. Even, *Chem. Phys. Lett.* 133 (1987) 59.
- [27] J. Sato, H. Kobayashi, Y. Inoue, *J. Phys. Chem. B* 107 (2003) 7970.



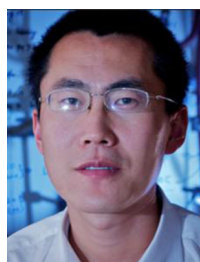
Xiaoqiang Du is pursuing his Ph.D. degree under the supervision of Prof. Yong Ding at the College of Chemistry and Chemical Engineering, Lanzhou University. He received his bachelor degree at Xinzhou Normal University in 2011. His current research focuses on design and modification of photocatalysis for water splitting.



Jinli Zhao received her bachelor degree in Chemistry from Tianshui Normal University in 2012. She is currently a Physical Chemistry Master's degree candidate in College of Chemistry and Chemical Engineering, Lanzhou University under the supervision of Prof. Yong Ding. Her research interests are focusing on solar energy photocatalytic hydrogen production catalyzed by polyoxometalates.



Jiaqi Mi Received her B.S. at Shandong University. She has been trained in chemical biology and synthetic chemistry for medicine application in Georgia State University and Emory University. Currently her research interest focuses on nanomaterials for bio-nano interface and anticancer nanomedicine development.



Yong Ding obtained the Ph.D. degree in Physical Chemistry from Lanzhou Institute of Chemical Physics, Chinese Academy of Sciences in 2005. After then, he joined Lanzhou University and was appointed as Associate Professor in College of Chemistry and Chemical Engineering. From 2009 to 2010, he was studying in Emory University as visiting scholar. In 2011, he was promoted to professor and doctoral supervisor. His

current research interest is focused on water splitting including water oxidation and water reduction. The catalysts are based on polyoxometalates, metal complex and metal oxides. Another field is the synthesis, characterization and catalytic performance of polyoxometalates.



Panpan Zhou obtained his Ph.D. (physical chemistry) degree at Lanzhou University in 2010. From 2010 to 2012, he did his postdoc with Prof. Tonglei Li at the College of Pharmacy, University of Kentucky. He then worked with Prof. Ruiqin Zhang at the Beijing Computational Science Research Center (CSRC) from 2012 to 2013. He joined the faculty of Lanzhou University in 2013. His research focuses on weak intermolecular interactions

in complex chemical or biological systems, conceptual density functional theory (CDFT) in chemical reaction mechanism.



Baochun Ma obtained the Ph.D. degree in Organic Chemistry from Lanzhou University in 2005. After then, she joined Lanzhou University and was appointed as Lecture in College of Chemistry and Chemical Engineering. From 2009 to 2010, she was studying in Emory University as visiting scholar. In 2010, she was promoted to Associate Professor. Her current research interest is focused on total synthesis of natural products and organic synthesis chemistry.



Junwei Zhao obtained the B.S. degree in chemistry in 2002 from Henan University and gained his MS degree in 2005 from Henan University. In 2008, he received his Ph.D. at Fujian Institute of Research on the Structure of Matter, Chinese Academy of Sciences. After then, he joined Henan University and was appointed as a Lecture. In 2010, he was promoted to an associate professor. In 2014, he was promoted to a professor and doctoral supervisor. His current research interest is focused on the synthesis and preparative chemistry of polyoxometalate-based functional materials and the relevant optical, electrical, magnetic and medical properties.



Jie Song trained at Emory University in Chemistry and Materials Science focusing on synthesis and catalysis of functional materials on both molecular and nanoscale levels. His research interests centered on engineering of new nanostructured materials for solar energy conversion and storage, environmental decontamination, as well as targeted nanomedicines for diagnosis and treatment of diseases (cancer, neurodegenerative disease, and HIV/AIDS). He is currently in the joint biomedical engineering department at Georgia Institute of Technology and Emory University working on the biological inspired synthesis of molecular semiconductors and porous nanomaterials for artificial photosynthesis and targeted drug delivery for cancer imaging and treatments.